Journal of Bioscience and Bioengineering
VOL. 125 No. 2, 251–257, 2018

www.elsevier.com/locate/jbiosc

Improved kinetic model of *Escherichia coli* central carbon metabolism in batch and continuous cultures

Hiroyuki Kurata[1,2,*] and Yurie Sugimoto[1]

Department of Bioscience and Bioinformatics, Kyushu Institute of Technology, 680-4 Kawazu, Iizuka, Fukuoka 820-8502, Japan[1] *and Biomedical Informatics R&D Center, Kyushu Institute of Technology, 680-4 Kawazu, Iizuka, Fukuoka 820-8502, Japan*[2]

Received 8 July 2017; accepted 16 September 2017
Available online 18 October 2017

Many kinetic models of *Escherichia coli* central metabolism have been built, but few models accurately reproduced the dynamic behaviors of wild type and multiple genetic mutants. In 2016, our latest kinetic model improved problems of existing models to reproduce the cell growth and glucose uptake of wild type, Δ*pykA*:*pykF* and Δ*pgi* in a batch culture, while it overestimated the glucose uptake and cell growth rates of Δ*ppc* and hardly captured the typical characteristics of the glyoxylate and TCA cycle fluxes for Δ*pgi* and Δ*ppc*. Such discrepancies between the simulated and experimental data suggested biological complexity. In this study, we overcame these problems by assuming critical mechanisms regarding the OAA-regulated isocitrate dehydrogenase activity, *aceBAK* gene regulation and growth suppression. The present model accurately predicts the extracellular and intracellular dynamics of wild type and many gene knockout mutants in batch and continuous cultures. It is now the most accurate, detailed kinetic model of *E. coli* central carbon metabolism and will contribute to advances in mathematical modeling of cell factories.

[**Key words:** Kinetic model; Synthetic biology; Central carbon metabolism; Dynamic simulation; *Escherichia coli*]

Systems biology and synthetic biology aim to understand the mechanism by which a biochemical network yields dynamic behaviors in response to environmental stresses or genetic variations and to rationally design and engineer such networks. Mathematical modeling is a powerful method that simulates biological behaviors and characteristics under different culture and genetic conditions. Different types of mathematical equations are available. S-system and General Mass Action are suitable when there are few kinetic data. In the case of widely-used microbes such as *Escherichia coli*, detailed Michaelis–Menten type equations have been developed for enzyme reactions in biochemistry and biochemical engineering. Kinetic models of *E. coli* central metabolism, including glycolysis, the tricarboxylic acid (TCA) cycle, the pentose phosphate pathway, the glyoxylate cycle, and anaplerotic pathways, have been built in a batch culture (1–5). Since metabolite and enzyme concentrations vary over time and with a change in environmental and genetic conditions, the models needed to integrate transcription factors, enzyme modification and allosteric reactions into the central carbon metabolism (6–10).

However, few kinetic models accurately reproduced the dynamic behaviors of wild type (WT) and multiple genetic mutants due to biological complexity. In 2016, we employed extensive parameter optimization by a supercomputer to build a detailed, accurate kinetic model for the central carbon metabolism with four transcriptional factors of *E. coli* in a batch culture (6). This kinetic model more accurately reproduced the cell growth and glucose uptake of WT, *pykA*:*pykF* knockout mutant (Δ*pykA*:*pykF*) and *pgi* knockout mutant (Δ*pgi*) in a batch culture than the existing models (1,3,7–9), while it remains to be improved. It overestimated the glucose uptake and cell growth rates of *ppc* knockout mutant (Δ*ppc*) and hardly captured the typical characteristics of the glyoxylate and TCA cycle fluxes for Δ*pgi* and Δ*ppc*. Such discrepancies between the simulated and experimental data suggested biological complexity.

To reproduce the dynamics and typical characteristics of the *E. coli* cells under different genetic and culture conditions, we improved our previous model (6) by assuming some mechanisms regarding the OAA-regulated isocitrate dehydrogenase (Icdh) activity, *aceBAK* gene regulation and cell growth suppression. The present or improved model estimated not only the extracellular dynamics but also the intracellular characteristics of WT and many genetic mutants in batch and continuous cultures.

MATERIALS AND METHODS

Kinetic model To solve some problems of our previous (Jahan) model (6), we have developed a kinetic model of the central carbon metabolism of *E. coli*, including the glycolytic pathway, pentose phosphate pathway, Entner–Doudoroff (ED) pathway, anaplerotic pathway, TCA cycle, glyoxylate cycle and oxidative phosphorylation, together with transcription factors of catabolite repressor/activator (Cra), cAMP receptor protein (Crp), pyruvate dehydrogenase complex repressor (PdhR), and acetate operon repressor (IclR), as shown in Fig. 1.

The following kinetic models are employed for batch and continuous cultures:

$$\frac{dX}{dt} = \mu(\mathbf{x}_1, \mathbf{x}_2, \mathbf{y}, \mathbf{p})X - DX \quad (1)$$

* Corresponding author at: Department of Bioscience and Bioinformatics, Kyushu Institute of Technology, 680-4 Kawazu, Iizuka, Fukuoka 820-8502, Japan. Tel./fax: +81 948 29 7828.
E-mail address: kurata@bio.kyutech.ac.jp (H. Kurata).

1389-1723/$ – see front matter
https://doi.org/10.1016/j.jbiosc.2017.09.005

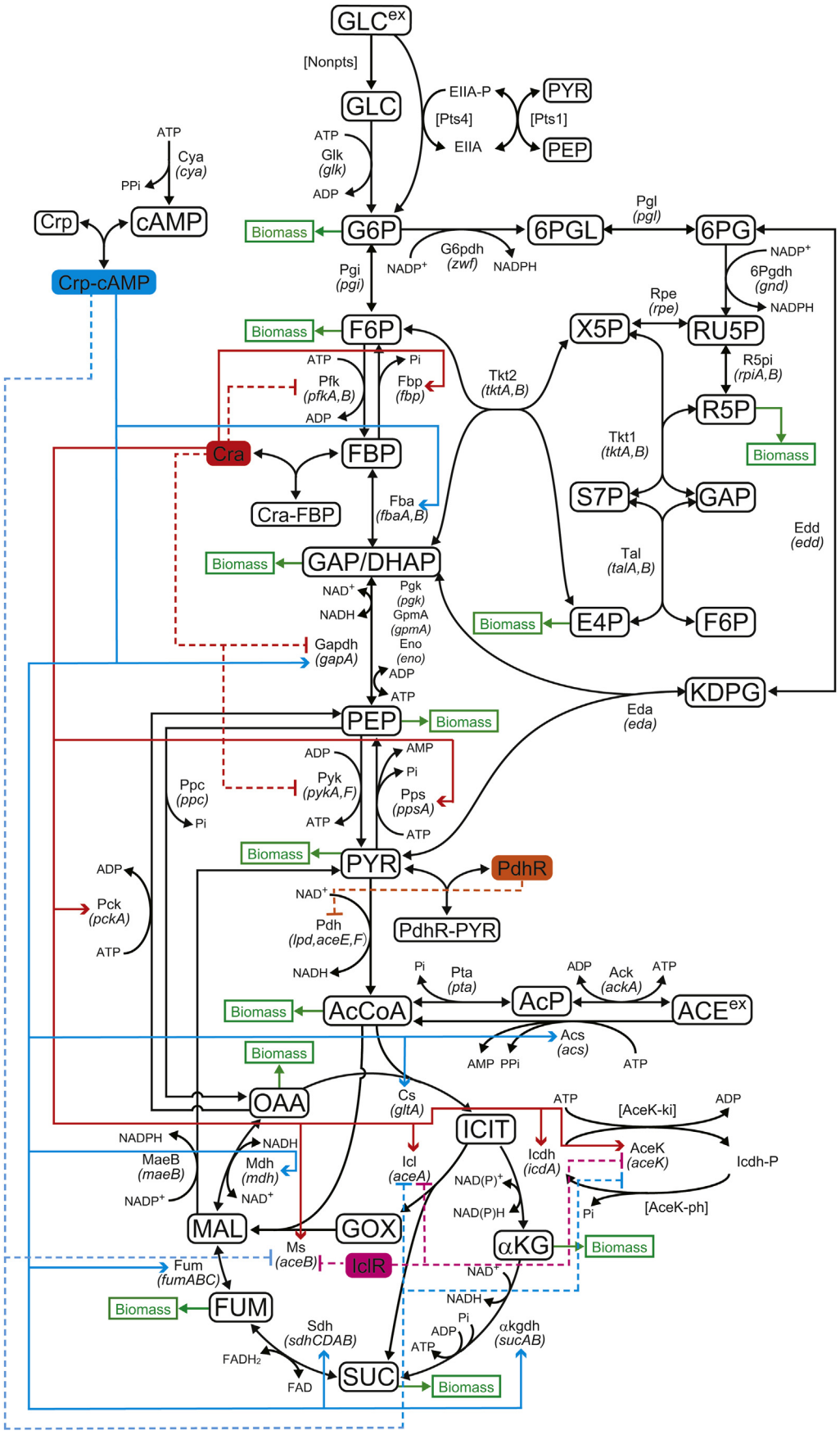

FIG. 1. An *E. coli* metabolic network map. The solid line indicates activation and the dotted line indicates repression.

$$\frac{d\mathbf{y}}{dt} = D\left(\mathbf{y}_{feed} - \mathbf{y}\right) - \mathbf{g}(\mathbf{x}_1, \mathbf{x}_2, \mathbf{y}, \mathbf{p})X \quad (2)$$

$$\frac{d\mathbf{x}_1}{dt} = \mathbf{f}(\mathbf{x}_1, \mathbf{x}_2, \mathbf{y}, \mathbf{p}) \quad (3)$$

$$\mathbf{x}_2 = \mathbf{h}(\mathbf{x}_1, \mathbf{y}, \mathbf{p}) \quad (4)$$

The equations show the dynamics of a batch culture when dilution rate D is set to zero. X is the cell concentration in a reactor, $\mathbf{x}_1$ is the vector of 50 time-varying molecule (metabolite, enzyme and proteins) concentrations, $\mathbf{x}_2$ is the vector of ancillary variables including intracellular transcription factor (TF) and TF-metabolite complex concentrations, $\mathbf{y}$ is the vector of extracellular substrate (glucose and acetate) concentrations, $\mathbf{y}_{feed}$ is the substrate concentration vector of the feed $\mathbf{p}$ is the vector of 341 kinetic or constant parameters, $\mu(\mathbf{x}_1, \mathbf{x}_2, \mathbf{y}, \mathbf{p})$is the specific growth rate, $\mathbf{g}(\mathbf{x}_1, \mathbf{x}_2, \mathbf{y}, \mathbf{p})$ is the function vector of specific substrate (glucose and acetate) uptake rates, $\mathbf{f}(\mathbf{x}_1, \mathbf{x}_2, \mathbf{y}, \mathbf{p})$ is the function vector of mass balance equations with respect to $\mathbf{x}_1$and $\mathbf{h}(\mathbf{x}_1, \mathbf{y}, \mathbf{p})$ is the function vector that provides $\mathbf{x}_2$. Details of the mass balance equations, reaction rates and ancillary variables are described in Supplementary Tables S1–S3. The kinetic model contains 27 metabolites, 23 enzymes, 44 enzyme fluxes, 22 gene expressions and 12 biomass production rate equations of intracellular precursor metabolites. All molecule concentrations are represented in units of millimolar (mM). The initial concentrations and parameters are presented in Supplementary Tables S4–S6. In a continuous culture, the flux distributions were calculated at the steady state. When the simulated fluxes of some reactions oscillate, the values of time-average fluxes were used as the steady-state flux distribution. The model was programmed by Matlab2016a (The Mathworks). The proposed kinetic model (Matlab program) is freely available at our site: http://www.cadlive.jp/cadlive_main/Softwares/KineticModel/Ecolimetabolism.html.

Experimental data The experimental data in a batch culture (11), including cell growth, metabolite concentrations and metabolic fluxes, were used to build the kinetic model. The experimental data in a continuous culture (12,13) were employed to validate the model. The genetic mutant list of Ishii et al. (12) consists of 24 single gene deletion mutants of *galM*, *glk*, *pgm*, *pgi*, *pfkA*, *pfkB*, *fbp*, *fbaB*, *gapC*, *gpmA*, *gpmB*, *pykA*, *pykF*, *ppsA*, *zwf*, *pgl*, *gnd*, *rpe*, *rpiA*, *rpiB*, *tktA*, *tktB*, *talA* and *talB*. A *ppc* gene deletion mutant was analyzed by Kadir et al. (13). Out of the 25 mutants, *galM*, *pgm*, *gapC* and *gpmB* gene deletion mutants were omitted, because the proteins encoded by them were not included in the kinetic models.

Mathematical description of gene deletion mutants Mathematical knockout mutants were constructed, classifying metabolic enzymes into isozymes and enzyme complexes. When a gene deletion mutant has an alternative enzyme (including isozyme) to the deleted gene product, the reaction flux associated with the deleted gene is not zero. When the deleted gene product is one component of an enzyme complex, its flux also decreases to a significant extent. For deletion of the genes with an isozyme: *pfkA*, *pfkB*, *pykA*, *pykF*, *rpiA*, *rpiB*, *tktA*, *tktB*, *talA* and *talB*, the maximum velocity of the reaction associated with the deleted gene was set to a half. Note that the genes included in an enzyme complex were not described in the gene deletion list.

RESULTS

Model improvement The previous model (6) had been well optimized under the provided constraints and mechanisms, but it missed some typical dynamics of the TCA and glyoxylate cycles. Tuning of the kinetic parameter values could not further optimize the previous model. Thus, a mechanism-based extensive analysis was performed for model improvement. We improved the model as follows. The Icdh activity regulation and the *aceBAK* gene expression were improved by Eqs. S83, S84 and Eq. S115, respectively, in Supplementary Table S2. The Ppc reaction kinetics was revised by Eq. S80. Cell growth suppression was implemented by Eq. S195 in Supplementary Table S3. The biomass rate equations were simplified by Eqs. S169–S180. Then, the values of 351 kinetic parameters were estimated so that the model can reproduce the glucose uptake and cell growth of WT and multiple knockout mutants and capture the typical characteristic of the TCA and glyoxylate cycle fluxes.

Dynamics of WT and three gene deletion mutants To test whether the present or improved kinetic model can reproduce the experimental data, the cell growth and extracellular glucose/acetate concentrations of WT, Δ*pykA*:Δ*pykF*, Δ*pgi* and Δ*ppc* strains were simulated in a batch culture (Fig. 2). The intracellular metabolite/enzyme concentrations and metabolic fluxes were simulated (Supplementary Figs. S1 and S2). The time courses of the glucose concentration were consistent with the experimental data for WT and the three knockout mutants. The cell concentration increased with a decrease in glucose. The glucose uptake of Δ*pykA*:Δ*pykF* was almost the same as that of WT, while that of Δ*pgi* and Δ*ppc* was much delayed as observed in the experiment. The present model greatly improved the dynamics of the cell growth and glucose uptake of Δ*ppc*, compared to the previous model (6). Acetate was produced during the growth phase and consumed thereafter. Fig. 3 shows the intracellular flux distributions for WT and the knockout mutants. WT and Δ*pykA*:Δ*pykF* dominantly used the TCA cycle (Fig. 3A and B), while they hardly used the glyoxylate cycle, as observed in the experiment. Since the dissociation constant between isocitrate (ICIT) and the Icdh enzyme (14) was much smaller than that between ICIT and the Icl enzyme (15), ICIT was dominantly converted into α-ketoglutarate (αKG) of the TCA cycle, but not into glyoxylate (GOX) of the glyoxylate cycle.

The previous kinetic model provided little flux to the TCA and glyoxylate cycles for Δ*pgi* and Δ*ppc*, differing from the experimental observation (11,13). On the other hand, the present model improved both the fluxes of the TCA and glyoxylate cycles so that they can significantly flow (Fig. 3C and D), although the estimated fluxes were relatively smaller than the experimental data. Such low fluxes were caused by a low flux of Cs due to shortage of oxaloacetate (OAA) in Δ*pgi*. Since the experimental data of the flux distribution of Δ*ppc* are not available for a batch culture but for a continuous culture (13), we simulated the flux distribution of Δ*ppc* in a continuous culture with $D = 0.2\ \mathrm{h}^{-1}$. The simulated results (Fig. 3D) captured the Δ*ppc* typical characteristics that the TCA and glyoxylate cycles are both active, as observed in the experiment. To confirm the prediction accuracy of the present kinetic model in a batch culture, Table 1 shows the correlation coefficients between the simulated and experimental data for WT and the two knockout mutants. The present model showed higher correlation coefficients for WT and Δ*pgi* than the previous one (6), although it provided a little less correlation coefficient for Δ*pykA*:Δ*pykF*.

Validation of the improved kinetic model To validate the prediction accuracy of the present kinetic model, the present and previous kinetic models simulated the steady-state flux distributions of WT and 21 single gene knockout mutants in a continuous culture, and calculated the correlation coefficients between the simulated and experimental data (12,13), as shown in Table 2. Note that the employed experimental data were not used for model construction. For WT and 17 mutants of Δ*glk*, Δ*pgi*, Δ*pfkA*, Δ*pfkB*, Δ*fbp*, Δ*fbaB*, Δ*pykA*, Δ*pykF*, Δ*ppsA*, Δ*zwf*, Δ*rpiA*, Δ*rpiB*, Δ*tktA*, Δ*tktB*, Δ*talA*, Δ*talB* and Δ*ppc*, the present model more accurately reproduced the flux distributions than the previous one. For WT, a decrease in D decreased the correlation coefficient. At a low dilution rate of 0.2, the correlation coefficient of WT decreased to 0.86. The present model increased the correlation coefficients of almost all genetic mutants at low dilution rate of 0.2. It is noteworthy that the present model greatly improves the flux distribution of Δ*ppc*. The fluxes of some metabolites oscillated for Δ*pfkA*, Δ*pfkB* and Δ*ppsA*. It may be caused by a feedback loop of the Pts with nonlinearity of the glucose uptake flux with respect to extracellular glucose. For the deletion of the *zwf* gene responsible for the entry glucose-6-phosphate dehydrogenase (G6pdh) reaction of the pentose phosphate pathway, the present model provided a high correlation coefficient, while Δ*zwf* made most of the glucose uptake flux enter the glycolysis pathway. The flux distributions of WT and the 17 genetic mutants, which reproduced the experimental data, are illustrated in Supplementary Fig. S3. The

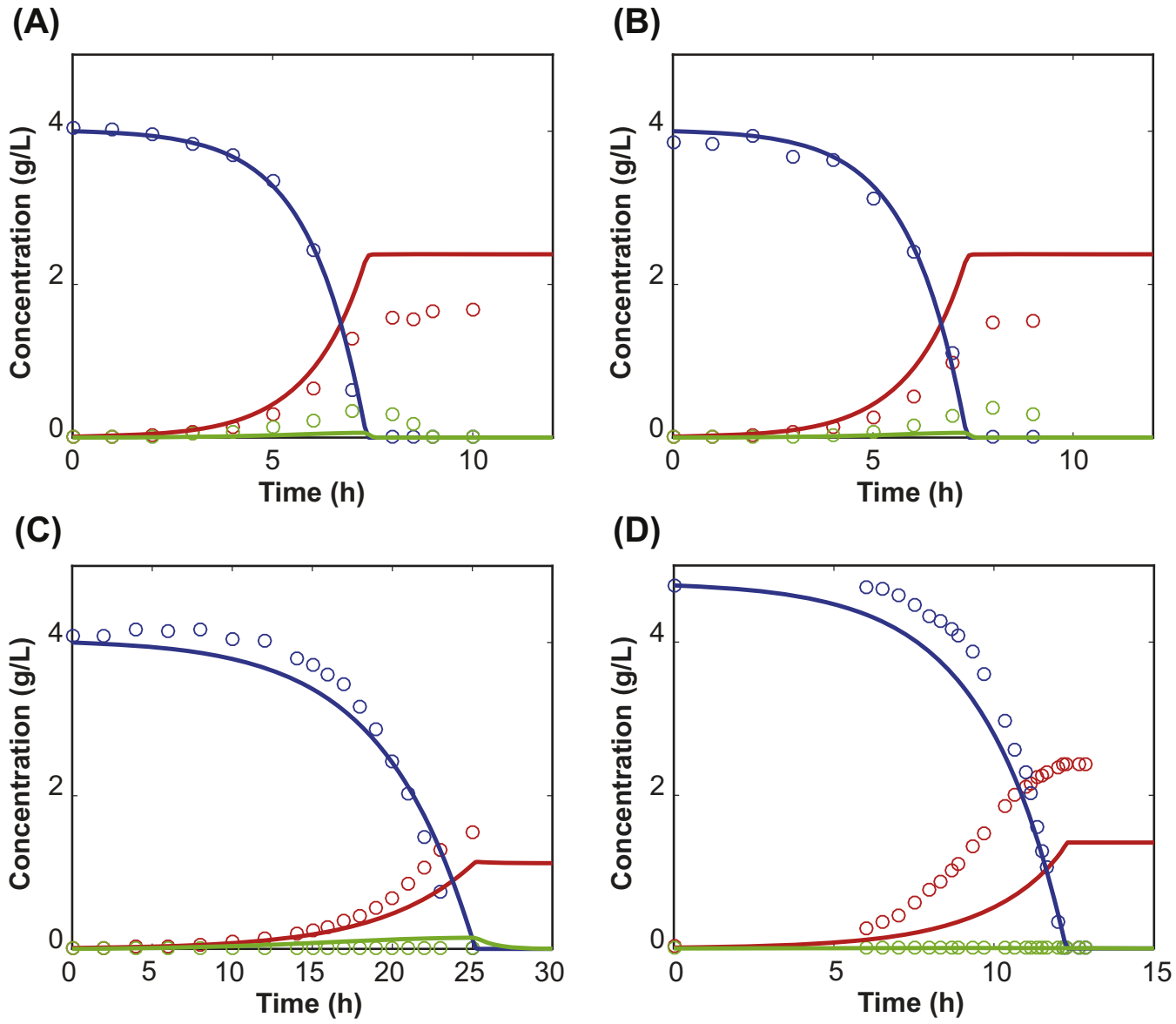

FIG. 2. The experimental validation of WT and gene knockout mutants in a batch culture. (A) WT. (B) Δ*pykA*:Δ*pykF*. (C) Δ*pgi*. (D) Δ*ppc*. The green, blue and red lines represent the simulation results of the extracellular glucose, biomass and acetate, respectively. The corresponding open circles represent the experimental data. (For interpretation of the references to colour in this figure legend, the reader is referred to the web version of this article.)

TCA and glyoxylate cycles flowed as observed in the experiments. The present model rather captured the characteristics of the TCA and glyoxylate cycle fluxes, although the previous one hardly produced those fluxes (data not shown). For 4 mutants of Δ*gpmA*, Δ*pgl*, Δ*gnd* and Δ*rpe*, the simulated fluxes of both the present and previous models disagreed with the experimental data. The reasons will be discussed later.

DISCUSSION

Developed model The previous kinetic model (6) had been the first model to our knowledge that reproduces the dynamics of multiple genetically modified mutants under an aerobic condition in a batch culture. It employs literature-based detailed kinetic equations with gene regulations to accurately reproduce experimental data for WT and multiple genetic mutants in a batch culture. However, it had some problems for predicting the flux distributions of the TCA and glyoxylate cycles and cell growth rates for some genetic mutants. The present model solved these problems. In addition, the model was demonstrated to predict the flux distributions of many gene deletion mutants more accurately than the previous one. The present model is now one of the most accurate, detailed kinetic models of *E. coli* central carbon metabolism. The following sections discuss the mechanisms of how the model is improved.

Backup of OAA by Icdh activity regulation In the previous model, the Cs flux for Δ*pgi* and Δ*ppc* was close to zero due to a low OAA concentration (Fig. S2 in the previous model), i.e., the TCA cycle was very suppressed. Since Δ*pgi* did not convert glucose 6-phosphate (G6P) into Fructose 6-phosphate (F6P) due to lack of phosphoglucose isomerase, it reduced the concentration of glycolytic metabolites: phosphoenolpyruvate (PEP), OAA and acetyl-CoA (AcCoA), resulting in suppressed TCA cycle. Since the

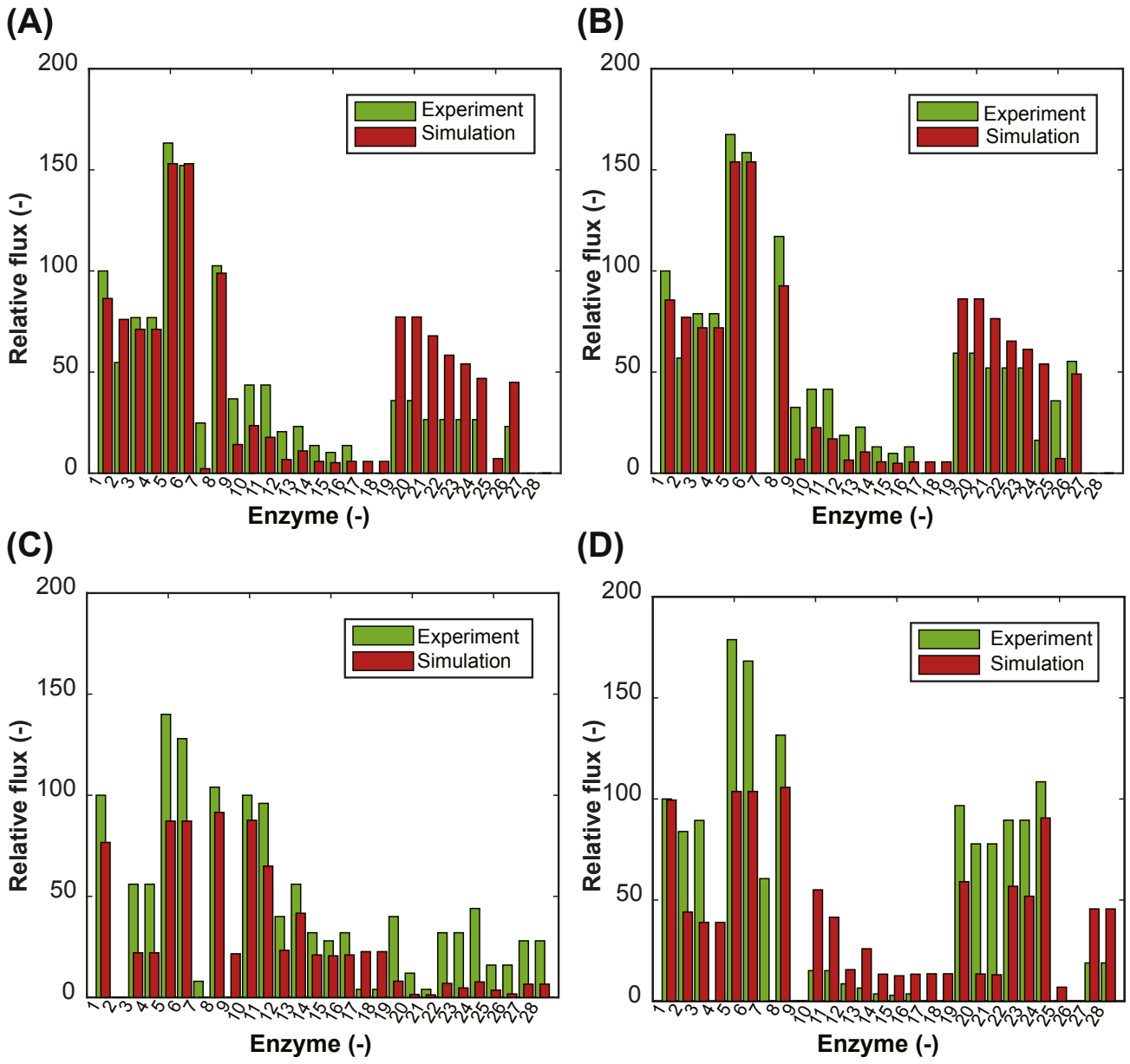

FIG. 3. Flux distributions for WT and gene knockout mutants in batch and continuous cultures. (A) WT, flux distribution on 5 h in a batch culture. (B) Δ*pykA*:Δ*pykF*, on 5 h in a batch culture. (C) Δ*pgi*, on 16 h in a batch culture. (D) Δ*ppc*, the steady-state flux distribution in a continuous culture at $D = 0.2\ h^{-1}$. The total glucose uptake flux (the sum of the Pts4 and non-Pts fluxes) was normalized as 100. The indexes indicate the enzymes. 1: vE_Pts4, 2: vE_Pgi, 3: vE_Pfk-vE_Fbp, 4: vE_Fba, 5: vE_Pgk, 6: vE_Eno, 7: vE_Pyk-vE_Pps, 8: vE_Pdh, 9: vE_Ack, 10: vE_G6pdh, 11: vE_6Pgdh, 12: vE_R5pi, 13: vE_Rpe, 14: vE_Tkt1, 15: vE_Tkt2, 16: vE_Tal, 17: vE_Edd, 18: vE_Eda, 19: vE_Cs, 20: vE_Icdh, 21: vE_αkgdh, 22: vE_Sdh, 23: vE_Fum, 24: vE_Mdh, 25: vE_MaeB, 26: vE_Ppc-vE_Pck, 27: vE_Icl, 28: vE_Ms. (vE shows a metabolic flux).

TABLE 1. Validation of the present kinetic model by the experimental fluxes in a batch culture.

Species	Sampling time (h)	Improved, present model		Previous model	
		Correlation coefficient	p-value	Correlation coefficient	p-value
WT	5	0.89	5.3E-10	0.99	5.8E-21
	6	0.97	7.2E-17	0.96	5.9E-15
	7	0.98	1.2E-19	0.94	4.2E-13
Δ*pykA*:Δ*pykF*	5	0.92	5.4E-12	0.98	1.0E-18
	6	0.90	2.6E-10	0.98	3.8E-18
	7	0.90	1.9E-10	0.98	2.1E-18
Δ*pgi*	16	0.92	9.9E-12	0.91	4.1E-11
	21	0.86	1.0E-08	0.83	9.7E-08
	23	0.78	1.9E-06	0.75	5.7E-06

Δ*ppc* does not supply OAA from PEP due to lack of phosphoenolpyruvate carboxylase (Ppc), decreasing the Cs reaction, Δ*ppc* provided null flux of the TCA cycle. However, those simulated results were inconsistent with the experimental observation that the TCA cycle actively proceeds for both Δ*pgi* and Δ*ppc*.

To solve this discrepancy under the employed network architecture, it is required to supply OAA in Δ*pgi* and Δ*ppc*, because the TCA cycle does not proceed without any sufficient supply of OAA. To backup OAA while making the TCA cycle function, it would be essential to effectively use the glyoxylate cycle. ICIT is a branch point for two pathways: the Icdh reaction of the TCA cycle and isocitrate lyase (Icl) reaction of the glyoxylate cycle. The Icdh activity, which is regulated by the *aceK* gene-encoding isocitrate dehydrogenase

TABLE 2. Validation of the kinetic model by the experimental fluxes in a continuous culture.

Deleted gene	Dilution rate (h^{-1})	Improved, present model		Previous model		Notes
		Correlation coefficient	p-value	Correlation coefficient	p-value	
glk	0.2	**0.76**	2.6E-08	0.54	5.3E-04	
pgi	0.2	**0.77**	1.5E-08	**0.74**	1.9E-07	
pfkA	0.2	**0.75**	8.1E-08	0.59	1.2E-04	OSC
pfkB	0.2	**0.80**	1.6E-09	0.68	3.0E-06	OSC
fbp	0.2	**0.83**	9.1E-11	0.61	5.7E-05	
fbaB	0.2	**0.82**	4.6E-10	0.65	1.4E-05	
gpmA	0.2	−0.22	1.9E-01	0.02	8.9E-01	DIS
pykA	0.2	**0.83**	1.6E-10	0.64	2.3E-05	
pykF	0.2	**0.89**	8.5E-14	**0.74**	2.0E-07	
ppsA	0.2	**0.78**	6.5E-09	0.64	1.7E-05	OSC
zwf	0.2	**0.90**	9.7E-15	**0.80**	2.9E-09	
pgl	0.2	0.20	2.2E-01	−0.16	3.5E-01	DIS
gnd	0.2	0.24	1.5E-01	0.28	9.7E-02	DIS
rpe	0.2	0.16	3.3E-01	−0.15	3.8E-01	DIS
rpiA	0.2	**0.83**	8.7E-11	0.55	4.4E-04	
rpiB	0.2	**0.80**	1.6E-09	0.56	3.0E-04	
tktA	0.2	**0.72**	3.1E-07	0.43	8.4E-03	
tktB	0.2	**0.74**	9.4E-08	0.57	2.5E-04	
talA	0.2	**0.76**	3.6E-08	0.60	1.0E-04	
talB	0.2	**0.76**	4.0E-08	0.57	2.0E-04	
ppc	0.2	**0.79**	1.0E-06	0.54	4.8E-03	13
WT	0.7	**0.95**	5.0E-20	**0.84**	5.3E-11	
WT	0.5	**0.94**	1.2E-18	**0.84**	8.5E-11	
WT	0.4	**0.90**	6.4E-15	**0.84**	1.1E-10	
WT	0.2	**0.86**	4.4E-12	**0.71**	8.9E-07	

DIS, simulated results disagree with experimental ones. OSC, some metabolite concentrations oscillate. Correlation coefficients of >0.7 are marked in bold.

kinase/phosphatase (AceK), is key to determine whether the glyoxylate cycle is activated. The Icdh is an active form and the phosphorylated Icdh is an inactive form. AceK is a bifunctional enzyme whose activity is controlled by many metabolite effectors. When OAA is a suppressive effector of kinase of AceK and an inductive effector of phosphatase of AceK, we assumed that AceK regulates the Icdh activity in nonlinear, sharp manner with respect to OAA. This assumption was implemented by adjusting the values of some kinetic parameters of Eqs. S83, S84 (Supplementary Table S2). Consequently, a low OAA concentration decreased the Icdh activity and then accumulated ICIT (Supplementary Fig. S1). ICIT was dominantly converted by Icl into the glyoxylate cycle, which supplied OAA to initiate the TCA cycle flux. On the contrary, a high OAA concentration increased the Icdh activity, resulting in the activation of the TCA cycle and repression of the glyoxylate cycle.

In general the glyoxylate cycle bypasses the decarboxylation steps that take place in the TCA cycle when complex sources such as glucose are not available. In terms of metabolic pathway analysis, we hypothesized that the OAA-regulated glyoxylate cycle functions when the anaplerotic (Ppc) pathway does not supply OAA to the TCA cycle or OAA is depleted. A low concentration of OAA increases the phosphorylation activity of AceK, deactivating the Icdh activity, which results in the enhanced Icl flux. To our limited knowledge, this hypothesis has not been raised before. To experimentally validate it, it is necessary to demonstrate how a change in OAA regulates the Icdh activity.

Regulation of *aceBAK* gene expression The kinetic model of Δ*pgi* decreased cAMP, fructose 1,6-biphosphate (FBP) and pyruvate (PYR), activating the expression of the *aceBAK* genes encoding Icl, malate synthase (Ms) and AceK, compared to WT, as observed in the experiments. On the contrary, the Δ*ppc* model increased those effectors to suppress the *aceBAK* gene expression. The simulated behaviors of Δ*ppc* were opposite to those for of Δ*pgi*. This was a serious problem of the previous kinetic model, because it represses the glyoxylate cycle of Δ*ppc* and fails to backup OAA. To solve this problem, the present model assumed that the growth suppression enhances the *aceBAK* gene expression according to the experimental observation (16), as shown in Eq. S115. Consequently, a decrease in the Icl and Ms enzymes was avoided in Δ*ppc* (Supplementary Fig. S1), so that the TCA and glyoxylate cycles flow.

Ppc reaction kinetics In Δ*pgi* of the previous model, a decrease in PEP remarkably repressed the Ppc reaction, resulting in the shortage of OAA. To conserve the Ppc flux in Δ*pgi*, as shown in Supplementary Fig. S2, the kinetic parameters of the Ppc reaction (Eq. S80) were improved to supply OAA at low PEP.

Growth suppression mechanism The previous model of Δ*ppc* provided little fluxes of the TCA fluxes and enhanced the glucose uptake rate due to accumulated PEP. If the model is revised to induce the TCA fluxes, the cell growth of Δ*ppc* will be much accelerated by the increased ATP production (Fig. 3D), which is opposed to experimental observation. Thus, some growth suppression mechanisms were supposed to be hidden in Δ*ppc*. Since sugar-phosphate was reported to suppress cell growth (17), the present model implemented an empirical, plain equation assuming sugar phosphate-suppressed cell growth (Eq. S195). While detailed mechanisms of the growth suppression remains to be revealed yet, this empirical equation was feasible to reproduce the experimental cell growth. Addition of the growth suppression mechanism was able to adjust the Icdh activity (Eqs. S83, S84), *aceBAK* gene expression (Eq. S115) and the Ppc reaction kinetics (Eq. 80) so that the model can rather reproduce the TCA and glyoxylate cycle flux distribution of WT and genetic mutants. This assumption was critically important for reproduction of cell growth suppression for Δ*ppc*.

Remaining discrepancy between the simulated and experimental results We discussed some reasons why the four mutants disagreed with the experimental data. In Δ*pgl*, the end metabolite product, 6PGL, which is caused by gene deletion, was extremely accumulated in simulation. The flux of the enzyme producing 6PGL, i.e., the entry flux of the pentose phosphate pathway disappeared or was extinguished, which deteriorated the simulated flux distribution. In Δ*gnd* and Δ*rpe*, 6PG and RU5P, were also greatly accumulated, respectively, although the ED pathway connected 6PG to glycolysis. It is because the ED pathway flux is small. In the model, the ED pathway enzymes were constitutively synthesized at a low level based on the experimental data that they were not detectable for WT and many genetic mutants. To reproduce the experimental dynamics of Δ*gnd* and Δ*rpe*, some assumptions are necessary that the ED pathway is activated in a pentose phosphate pathway-related gene deletion mutant and that the entry flux of the pentose phosphate pathway is suppressed. The experimental flux distribution of Δ*gpmA* hardly changed compared with that of WT, but the simulated distribution remarkably changed. In our model, Δ*gpmA* separated the central carbon network into the upper part including glycolysis and the pentose phosphate pathway and the lower part with the TCA cycle, while both the parts are weakly connected through the ED pathway. This separation deteriorated the network structure and its kinetics because of a low activity of the ED pathway. To solve these problems, the kinetic model needs to incorporate alternative metabolic pathways compensating the deletion of *gpmA*.

Supplementary data related to this article can be found at https://doi.org/10.1016/j.jbiosc.2017.09.005.

ACKNOWLEDGMENTS

This work was supported by a Grant-in-Aid for Scientific Research (B) (16H02898) from the Japan Society for the Promotion of Science (JSPS) and was partially supported by the developing key technologies for discovering and manufacturing pharmaceuticals

used for next-generation treatments and diagnoses both from the Ministry of Economy, Trade and Industry, Japan (METI) and from Japan Agency for Medical Research and Development (AMED).

References

1. **Khodayari, A. and Maranas, C. D.:** A genome-scale *Escherichia coli* kinetic metabolic model k-ecoli457 satisfying flux data for multiple mutant strains, Nat. Commun., **7**, 13806 (2016).
2. **Kurata, H., Maeda, K., and Matsuoka, Y.:** Dynamic modeling of metabolic and gene regulatory systems toward developing virtual microbes, J. Chem. Eng. Jpn., **47**, 1–9 (2014).
3. **Chassagnole, C., Noisommit-Rizzi, N., Schmid, J. W., Mauch, K., and Reuss, M.:** Dynamic modeling of the central carbon metabolism of *Escherichia coli*, Biotechnol. Bioeng., **79**, 53–73 (2002).
4. **Visser, D., Schmid, J. W., Mauch, K., Reuss, M., and Heijnen, J. J.:** Optimal re-design of primary metabolism in *Escherichia coli* using linlog kinetics, Metab. Eng., **6**, 378–390 (2004).
5. **Costa, R. S., Machado, D., Rocha, I., and Ferreira, E. C.:** Hybrid dynamic modeling of *Escherichia coli* central metabolic network combining Michaelis-Menten and approximate kinetic equations, Biosystems, **100**, 150–157 (2010).
6. **Jahan, N., Maeda, K., Matsuoka, Y., Sugimoto, Y., and Kurata, H.:** Development of an accurate kinetic model for the central carbon metabolism of *Escherichia coli*, Microb. Cell Fact., **15**, 112 (2016).
7. **Usuda, Y., Nishio, Y., Iwatani, S., Van Dien, S. J., Imaizumi, A., Shimbo, K., Kageyama, N., Iwahata, D., Miyano, H., and Matsui, K.:** Dynamic modeling of *Escherichia coli* metabolic and regulatory systems for amino-acid production, J. Biotechnol., **147**, 17–30 (2010).
8. **Matsuoka, Y. and Shimizu, K.:** Catabolite regulation analysis of *Escherichia coli* for acetate overflow mechanism and co-consumption of multiple sugars based on systems biology approach using computer simulation, J. Biotechnol., **168**, 155–173 (2013).
9. **Kotte, O., Zaugg, J. B., and Heinemann, M.:** Bacterial adaptation through distributed sensing of metabolic fluxes, Mol. Syst. Biol., **6**, 355 (2010).
10. **Matsuoka, Y. and Kurata, H.:** Modeling and simulation of the redox regulation of the metabolism in *Escherichia coli* at different oxygen concentrations, Biotechnol. Biofuels, **10**, 183 (2017).
11. **Toya, Y., Ishii, N., Nakahigashi, K., Hirasawa, T., Soga, T., Tomita, M., and Shimizu, K.:** 13C-metabolic flux analysis for batch culture of *Escherichia coli* and its Pyk and Pgi gene knockout mutants based on mass isotopomer distribution of intracellular metabolites, Biotechnol. Prog., **26**, 975–992 (2010).
12. **Ishii, N., Nakahigashi, K., Baba, T., Robert, M., Soga, T., Kanai, A., Hirasawa, T., Naba, M., Hirai, K., Hoque, A., and other 19 authors:** Multiple high-throughput analyses monitor the response of *E. coli* to perturbations, Science, **316**, 593–597 (2007).
13. **Kadir, T. A., Mannan, A. A., Kierzek, A. M., McFadden, J., and Shimizu, K.:** Modeling and simulation of the main metabolism in *Escherichia coli* and its several single-gene knockout mutants with experimental verification, Microb. Cell Fact., **9**, 88 (2010).
14. **Garnak, M. and Reeves, H. C.:** Purification and properties of phosphorylated isocitrate dehydrogenase of *Escherichia coli*, J. Biol. Chem., **254**, 7915–7920 (1979).
15. **MacKintosh, C. and Nimmo, H. G.:** Purification and regulatory properties of isocitrate lyase from *Escherichia coli* ML308, Biochem. J., **250**, 25–31 (1988).
16. **Peng, L., Arauzo-Bravo, M. J., and Shimizu, K.:** Metabolic flux analysis for a *ppc* mutant *Escherichia coli* based on 13C-labelling experiments together with enzyme activity assays and intracellular metabolite measurements, FEMS Microbiol. Lett., **235**, 17–23 (2004).
17. **Kadner, R. J., Murphy, G. P., and Stephens, C. M.:** Two mechanisms for growth inhibition by elevated transport of sugar phosphates in *Escherichia coli*, J. Gen. Microbiol., **138**, 2007–2014 (1992).